Research Article Vol. 26, No. 10 | 14 May 2018 | OPTICS EXPRESS 12838

Optics EXPRESS

Theoretical design of twelve-band infrared metamaterial perfect absorber by combining the dipole, quadrupole, and octopole plasmon resonance modes of four different ring-strip resonators

LEI ZHAO, HAN LIU, ZHIHONG HE, AND SHIKUI DONG*

School of Energy Science and Engineering, Harbin Institute of Technology, Harbin 150001, China
*dongsk@hit.edu.cn

Abstract: Multiband metamaterial perfect absorbers (MPAs) have promising applications in many fields like microbolometers, infrared detection, biosensing, and thermal emitters. In general, the single resonator can only excite a fundamental mode and achieve single absorption band. The multiband MPA can be achieved by combining several different sized resonators together. However, it's still challenging to design the MPA with absorption bands of more than four and average absorptivity of more than 90% due to the interaction between differently sized resonators. In this paper, three absorption bands are successfully achieved with average absorptivity up to 98.5% only utilizing single one our designed ring-strip resonator, which can simultaneously excite a fundamental electric dipole mode, a higher-order electric quadrupole mode, and a higher-order electric octopole mode. As the biosensor, the sensing performance of the higher-order modes is higher than the fundamental modes. Then we try to increase the absorption bands by combining different sized ring-strip resonators together and make the average absorptivity above 90% by optimizing the geometry parameters. A six-band MPA is achieved by combining two different sized ring-strip resonators with average absorptivity up to 98.8%, which can excite two dipole modes, two quadrupole modes, and two octopole modes. A twelve-band MPA is achieved by combining four different sized ring-strip resonators with average absorptivity up to 93.7%, which can excite four dipole modes, four quadrupole modes, and four octopole modes.

OCIS codes: (160.3918) Metamaterials; (300.1030) Absorption; (310.6628) Subwavelength structures, nanostructures.

References and links

1. K. Chen, R. Adato, and H. Altug, "Dual-band perfect absorber for multispectral plasmon-enhanced infrared spectroscopy," ACS Nano **6**(9), 7998–8006 (2012).
2. N. Liu, M. Mesch, T. Weiss, M. Hentschel, and H. Giessen, "Infrared perfect absorber and its application as plasmonic sensor," Nano Lett. **10**(7), 2342–2348 (2010).
3. F. Bilotti, S. Tricarico, and L. Vegni, "Plasmonic metamaterial cloaking at optical frequencies," IEEE Trans. NanoTechnol. **9**(1), 55–61 (2010).
4. D. Schurig, J. J. Mock, B. J. Justice, S. A. Cummer, J. B. Pendry, A. F. Starr, and D. R. Smith, "Metamaterial electromagnetic cloak at microwave frequencies," Science **314**(5801), 977–980 (2006).
5. J. B. Pendry, "Negative refraction makes a perfect lens," Phys. Rev. Lett. **85**(18), 3966–3969 (2000).
6. N. Garcia and M. Nieto-Vesperinas, "Left-Handed Materials Do Not Make a Perfect Lens," Phys. Rev. Lett. **88**(20), 207403 (2002).
7. H. Li, S. Liu, S. Liu, S. Wang, G. Ding, H. Yang, and Z. Yu, "Low-loss metamaterial electromagnetically induced transparency based on electric toroidal dipolar response," Appl. Phys. Lett. **106**, 083511 (2015).
8. H. Zhang, Y. Cao, Y. Liu, Y. Li, and Y. Zhang, "Electromagnetically Induced Transparency Based on Cascaded π-Shaped Graphene Nanostructure," Plasmonics **12**(6), 1833–1839 (2017).
9. T. Maier and H. Brückl, "Wavelength-tunable microbolometers with metamaterial absorbers," Opt. Lett. **34**(19), 3012–3014 (2009).
10. T. Maier and H. Brueckl, "Multispectral microbolometers for the midinfrared," Opt. Lett. **35**(22), 3766–3768 (2010).

#325970 https://doi.org/10.1364/OE.26.012838
Journal © 2018 Received 13 Mar 2018; revised 22 Apr 2018; accepted 23 Apr 2018; published 3 May 2018

Optics EXPRESS

11. J. Grant, I. Escorcia-Carranza, C. Li, I. J. H. McCrindle, J. Gough, and D. R. S. Cumming, “A monolithic resonant terahertz sensor element comprising a metamaterial absorber and micro-bolometer,” Laser Photonics Rev. **7**(6), 1043–1048 (2013).
12. S. Ogawa, K. Okada, N. Fukushima, and M. Kimata, “Wavelength selective uncooled infrared sensor by plasmonics,” Appl. Phys. Lett. **100**(2), 021111 (2012).
13. S. Ogawa, K. Masuda, Y. Takagawa, and M. Kimata, “Polarization-selective uncooled infrared sensor with asymmetric two-dimensional plasmonic absorber,” Opt. Eng. **53**(10), 107110 (2014).
14. J. Y. Suen, K. Fan, J. Montoya, C. Bingham, V. Stenger, S. Sriram, and W. J. Padilla, “Multifunctional metamaterial pyroelectric infrared detectors,” Optics **4**, 276–279 (2017).
15. K. Q. Le, Q. M. Ngo, and T. K. Nguyen, “Nanostructured-Insulator-Metal Metamaterials for Refractive Index Biosensing Applications: Design, Fabrication, and Characterization,” IEEE J. Sel. Top. Quantum Electron. **23**(2), 388 (2017).
16. R. Li, D. Wu, Y. Liu, L. Yu, Z. Yu, and H. Ye, “Infrared Plasmonic Refractive Index Sensor with Ultra-High Figure of Merit Based on the Optimized All-Metal Grating,” Nanoscale Res. Lett. **12**(1), 1 (2017).
17. A. Karalis and J. D. Joannopoulos, “‘Squeezing’ near-field thermal emission for ultra-efficient high-power thermophotovoltaic conversion,” Sci. Rep. **6**(1), 28472 (2016).
18. D. Xiao and K. Tao, “Ultra-compact metamaterial absorber for multiband light absorption at mid-infrared frequencies,” Appl. Phys. Express **8**(10), 102001 (2015).
19. S. Ogawa, J. Komoda, K. Masuda, and M. Kimata, “Wavelength selective wideband uncooled infrared sensor using a two-dimensional plasmonic absorber,” Opt. Eng. **52**(12), 127104 (2013).
20. L. Meng, D. Zhao, Z. Ruan, Q. Li, Y. Yang, and M. Qiu, “Optimized grating as an ultra-narrow band absorber or plasmonic sensor,” Opt. Lett. **39**(5), 1137–1140 (2014).
21. X. Lu, L. Zhang, and T. Zhang, “Nanoslit-microcavity-based narrow band absorber for sensing applications,” Opt. Express **23**(16), 20715–20720 (2015).
22. J. W. Park, P. V. Tuong, J. Y. Rhee, K. W. Kim, W. H. Jang, E. H. Choi, L. Y. Chen, and Y. Lee, “Multi-band metamaterial absorber based on the arrangement of donut-type resonators,” Opt. Express **21**(8), 9691–9702 (2013).
23. N. Liu, H. Guo, L. Fu, S. Kaiser, H. Schweizer, and H. Giessen, “Plasmon hybridization in stacked cut-wire metamaterials,” Adv. Mater. **19**(21), 3628–3632 (2007).
24. J. Kim, K. Han, and J. W. Hahn, “Selective dual-band metamaterial perfect absorber for infrared stealth technology,” Sci. Rep. **7**(1), 6740 (2017).
25. S. Kang, Z. Qian, V. Rajaram, A. Alu, and M. Rinaldi, “Ultra narrowband infrared absorbers for omni-directional and polarization insensitive multi-spectral sensing microsystems,” Transducers 2017, Kaohsiung, TAIWAN, June 18–22, 2017.
26. J. Grant, M. Kenney, Y. D. Shan, I. Escorcia-Carranza, and D. R. S. Cumming, “CMOS compatible metamaterial absorbers for hyperspectral medium wave infrared imaging and sensing applications,” Opt. Express **26**(8), 10408–10420 (2018).
27. J. Le Perchec, Y. Desieres, N. Rochat, and R. Espiau De Lamaestre, “Subwavelength optical absorber with an integrated photon sorter,” Appl. Phys. Lett. **100**(11), 113305 (2012).
28. Y. Ma, Q. Chen, J. Grant, S. C. Saha, A. Khalid, and D. R. S. Cumming, “A terahertz polarization insensitive dual band metamaterial absorber,” Opt. Lett. **36**(6), 945–947 (2011).
29. M. Kenney, J. Grant, Y. D. Shah, I. Escorcia-Carranza, M. Humphreys, and D. R. S. Cumming, “Octave-Spanning Broadband Absorption of Terahertz Light Using Metasurface Fractal-Cross Absorbers,” ACS Photonics **4**(10), 2604–2612 (2017).
30. S. Fan and Y. Song, “Bandwidth-enhanced polarization-insensitive metamaterial absorber based on fractal structures,” J. Appl. Phys. **123**(8), 085110 (2018).
31. B. X. Wang, X. Zhai, G. Z. Wang, W. Q. Huang, and L. L. Wang, “Design of a four-band and polarization-insensitive terahertz metamaterial absorber,” IEEE Photonics J. **7**, 4600108 (2015).
32. D. Zheng, Y. Cheng, D. Cheng, Y. Nie, and R. Gong, “Four-Band Polarization-Insensitive Metama- Terial Absorber Based on Flower-Shaped Structures,” Prog. Electromagnetics Res. **142**, 221–229 (2013).
33. G. Dayal, A. Solanki, X. Yu Chin, T. C. Sum, C. Soci, and R. Singh, “High- Q plasmonic infrared absorber for sensing of molecular resonances in hybrid lead halide perovskites,” J. Appl. Phys. **122**(7), 073101 (2017).
34. X. Liu, J. Gao, H. Yang, X. Wang, and C. Guo, “Multiple infrared bands absorber based on multilayer gratings,” Opt. Commun. **410**, 438–442 (2018).
35. E. Aslan, S. Kaya, E. Aslan, S. Korkmaz, O. G. Saracoglu, and M. Turkmen, “Polarization insensitive plasmonic perfect absorber with coupled antisymmetric nanorod array,” Sens. Actuators B Chem. **243**, 617–625 (2017).
36. N. Liu, L. Langguth, T. Weiss, J. Kästel, M. Fleischhauer, T. Pfau, and H. Giessen, “Plasmonic analogue of electromagnetically induced transparency at the Drude damping limit,” Nat. Mater. **8**(9), 758–762 (2009).
37. C. Chen, Y. Sheng, and W. Jun, “Computed a multiple band metamaterial absorber and its application based on the figure of merit value,” Opt. Commun. **406**, 145–150 (2018).
38. N. Liu, M. Mesch, T. Weiss, M. Hentschel, and H. Giessen, “Infrared Perfect Absorber and its Application As Plasmonic Sensor,” Nano Lett. **10**(7), 2342–2348 (2010).

Optics EXPRESS

1. Introduction

Metamaterials (MM) usually possess some unique properties beyond the limitation of nature, which relies on the nanostructure rather than the chemical compositions. The MMs have exciting applications in many fields, such as perfect absorbers [1, 2], invisible cloaking [3, 4], perfect lenses [5, 6], and electromagnetically induced transparency [7, 8]. Among them, the metamaterial perfect absorbers (MPA) with nearly unity electromagnetic waves absorption characteristic have been intensively studied by many scientists due to their potential applications in microbolometers [9–11], infrared detection and imaging devices [12–14], biosensing [15, 16], and thermal emitters [17, 18]. Most MPAs are the triple-layered metal-dielectric-metal (MIM) configuration. The bottom metal block prohibits the transmission of electromagnetic waves. The top periodic metal resonators may lead to the excitation of localized plasmon resonances and the huge enhancement of the electric fields owing to the incident electromagnetic waves induced collective oscillations of the conduction electrons.

However, the MPAs based on the excitation of plasmon resonances have the common problem of single-band, which greatly limits its application especially for infrared detection and imaging devices. The detectors based on MPA can realize frequency-selective detection, which may decrease the disturbance of the environment and consequently increase the detection accuracy and resolution. But the single-band MPA based infrared detector generally can only respond to one infrared band thermal radiation. So if we want to achieve multiband detection by using the single-band MPA, it will need a series of detectors with different response wavelengths, which may lead to a complicated system [19]. The infrared detector based on multiband MPAs is a suitable solution to the above problem. For the multiband applications like sensing and detection, the design of the multiband metamaterial perfect absorber is highly desirable.

In general, one kind of metallic resonators can only get the single-band metamaterial perfect absorber [20], whose peak absorption wavelength is sensitive to the geometry parameters of the resonators and the refractive index of the dielectric and environment [19]. To achieve multiband absorption, a common and direct strategy is to combine several different sized resonators to get the super resonators [21–26]. Recently, researchers have achieved dual-band perfect absorption by combining two periodic nano-patch resonators [27] and square ring resonators [28], triple-band perfect absorption by using the fractals structure [29, 30], and quad-band perfect absorption by combining four periodic square ring resonators [31] and flower-shaped resonators [32]. In all the above structure, each kind of resonator corresponds to a plasmon resonance and an absorption peak. According to this logic, we can get as many as absorption bands as we want. Actually, it's impossible. For the super resonators consisting of four different sized resonators, the interaction between the adjacent resonators is already very strong and it is a great challenge to realize perfect absorption for the four absorption bands simultaneously. So the number of absorption bands of current metamaterial perfect absorbers is almost no more than four.

All the above mentioned multiband metamaterial perfect absorbers are based on the combination of fundamental plasmon resonances of different sized periodic metallic resonators. The strong interaction between the different resonators greatly limits the number of the perfect absorption bands. Actually, exciting higher-order plasmon resonance is a promising way to design multiband absorbers with perfect absorbance bands number greater than four. But the investigation of higher-order modes is rarely reported. Recently, some groups have done a few research about the higher-order resonances modes of periodic metallic structures like ring-rectangle cavity [33], Ag/Si multilayer grating [34], and four-fold triple-nanorods [35]. Although these structures can excite fundamental and higher-order modes at the same time and the fundamental modes can achieve nearly perfect absorption, the absorption magnitude of higher-order modes is usually less than 50% [33–35]. So it's challenging to achieve the absorptivity of the fundamental and higher-order modes greater than 90% simultaneously. What's more challenging is that achieving the absorptivity of all

Optics EXPRESS

the fundamental and higher-order modes greater than 90% simultaneously for a super resonator consisting of a few differently sized resonators.

In this paper, motivated by the above problems, the ring-strip structure is designed to excite the fundamental modes and higher-order modes simultaneously. By optimizing the geometry parameters, the average absorptivity of the fundamental modes and higher-order modes can be greater than 90%. The electric fields distribution is analyzed to figure out the underlying physical mechanism of the high absorptivity. It's also studied that the dependence of the absorption bands on the geometry parameters and the sensing performance of the fundamental and higher-order modes. The metamaterial perfect absorbers consisting of different sized ring-strip resonators are designed to make the absorption bands number greater than 4.

2. Design strategy and simulation method

Our designed metamaterial perfect absorber is the triple-layered metal-dielectric-metal (MIM) configuration. The bottom layer is the metal block and the middle layer is the dielectric block. The top layer is the periodic metal resonators. In general, one kind of resonator can only excite one mode (the fundamental mode) and obtain the single-band metamaterial perfect absorber. In order to achieve multiband absorption, a common and direct strategy is to combine several different sized resonators together to obtain the super resonators. However, the band numbers of the absorber are generally no more than four due to the interaction between differently sized resonators. The purpose of this paper is to design a perfect absorber with absorption bands of more than four and average absorptivity of more than 90%. Our design strategy is as follows. First of all, a basic resonator is designed by simulation, which can simultaneously excite the fundamental plasmon resonances and higher-order plasmon resonances. Through the parameters optimization, the average absorptivity of the basic resonator is designed to be more than 90%. Then the MPA based on the super resonators consisting of two or four different sized basic resonators are designed to make the absorption bands number greater than four. The average absorptivity of MPA is designed to be more than 90% through the parameters optimization. Finally, the perfect absorbers are successfully achieved with absorption bands of more than four and average absorptivity of more than 90%. The electromagnetic performance of our designed nanostructure is analyzed by the finite-difference-time-domain (FDTD) method. We only consider one unit cell in the simulation due to the periodicity of the structure. The periodic boundary condition is applied in the x- and y-direction and the PML boundary condition is applied in the z-direction.

Optics EXPRESS

3. Results and discussion

3.1 MPA based on the basic resonator with a fundamental mode and two higher-order modes

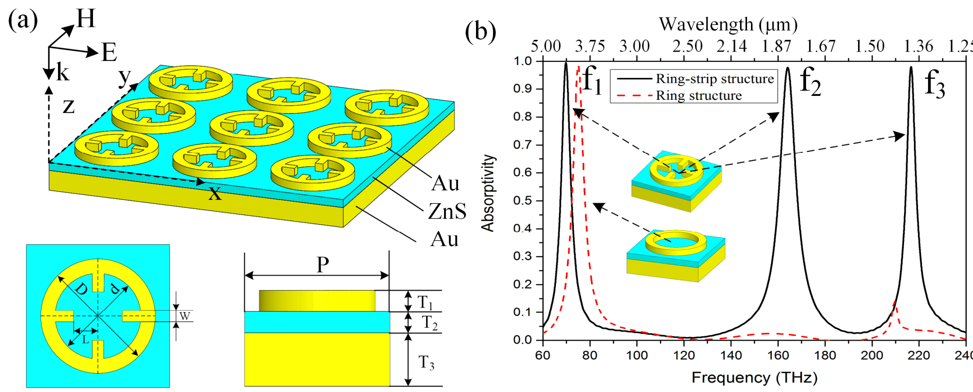

Fig. 1. (a) Schematic diagram of our designed MPA based on the basic resonators with a fundamental mode and two higher-order modes; (b) Spectral absorptivity of the basic ring-strip structure and the ring structure.

The schematic diagram of our designed basic resonator is shown in Fig. 1(a), which mainly consisting of triple layers. The bottom layer is the gold block with thickness T_3 and the middle layer is the ZnS block with thickness T_2. The top layer is the periodic ring-strip resonators with thickness T_1. The d and D indicate the inner and outer diameter of the ring. The W is the width of the strip. One end of the strip is connected to the ring, and the other end is at a distance L from the center of the ring. The electromagnetic waves are incident vertically on the nanostructure and the electric fields are polarized in the x-direction. In the simulation, the permittivity of Au is derived from Drude model $\varepsilon=1-\omega_p^2/\omega(\omega+i\gamma_0)$, where the plasmon frequency is $\omega_p=1.37\times10^{16}\,s^{-1}$ and the collision frequency is $\gamma_0=4.08\times10^{13}\,s^{-1}$ [36]. The permittivity of ZnS is 4.84 [37].

The optimized geometry parameters of the ring-strip structure used in the simulation are as follows: P = 0.6, T_1 = 0.05, T_2 = 0.05, T_3 = 0.2, d = 0.36, D = 0.5, W = 0.02, and L = 0.05 (units: μm). The spectral absorptivity of the ring-strip structure is shown in Fig. 1(b) with the solid black line. It's clear to see that there are three absorption peaks in the infrared frequency range at f_1 = 69.8 THz, f_2 = 164.1 THz, and f_3 = 216.6 THz with absorptivity 99.5%, 97.8%, and 98.1%, respectively. The average absorptivity of those three absorption peaks reaches 98.5%. We also investigate the ring structure and the spectral absorptivity is plotted in the Fig. 1(b) with the dash red line. Only one absorption peak appears in the infrared range at 75.1 THz as expected. So our designed ring-strip structure cannot only excite the fundamental model but also excite two extra higher-order modes compared to the ring structure. The average absorptivity of the fundamental model and higher-order modes exceed 90%, up to 98.5%.

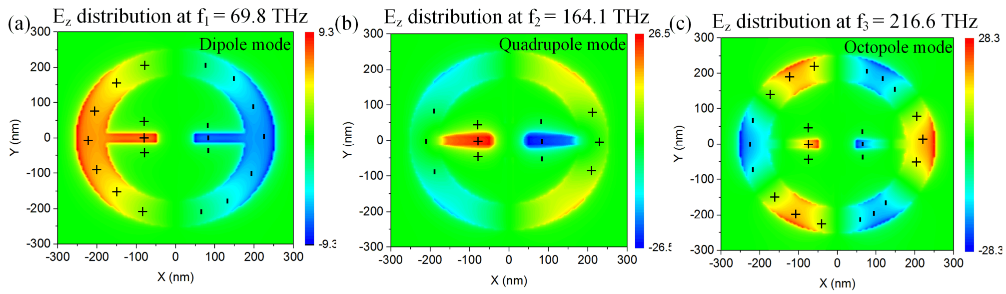

Fig. 2. The x-y cross-section view for the distribution of z component of electric fields E_z at (a) f_1 = 69.8 THz, (b) f_2 = 164.1 THz, and (c) f_3 = 216.6 THz.

To better understand the physical mechanism of the triple-band MPA based on the basic ring-strip resonators, the distribution of z component of electric fields E_z is plotted in Fig. 2. The E_z distribution can indicate the polarization charges distribution. The plus and minus signs in the figure indicate the distribution of the positive and negative charges. Figure 2(a) shows the E_z distribution at f_1 = 69.8 THz. This mode has two poles with equal magnitude but opposite signs. The charges mainly accumulate at the corners of the strips and the rings. Therefore, the absorption peak at f_1 = 69.8 THz comes from the excitation of electric dipole (ED) mode, which also called the fundamental mode. Figure 2(b) shows the E_z distribution at f_2 = 164.1 THz. This mode has four poles with equal magnitude, in which there are two positive poles and two negative poles. Therefore, the absorption peak at f_2 = 164.1 THz comes from the excitation of electric quadrupole (EQ) mode, which is the higher-order mode. Figure 2(c) shows the E_z distribution at f_3 = 216.6 THz. This mode has eight poles with equal magnitude, in which there are four positive poles and four negative poles. Therefore, the absorption peak at f_3 = 216.6 THz comes from the excitation of electric octopole (EO) mode, which is also the higher-order mode. So our designed ring-strip structure cannot only excite the fundamental electric dipole model but also excite two higher-order electric quadrupole and electric octopole modes.

Optics EXPRESS

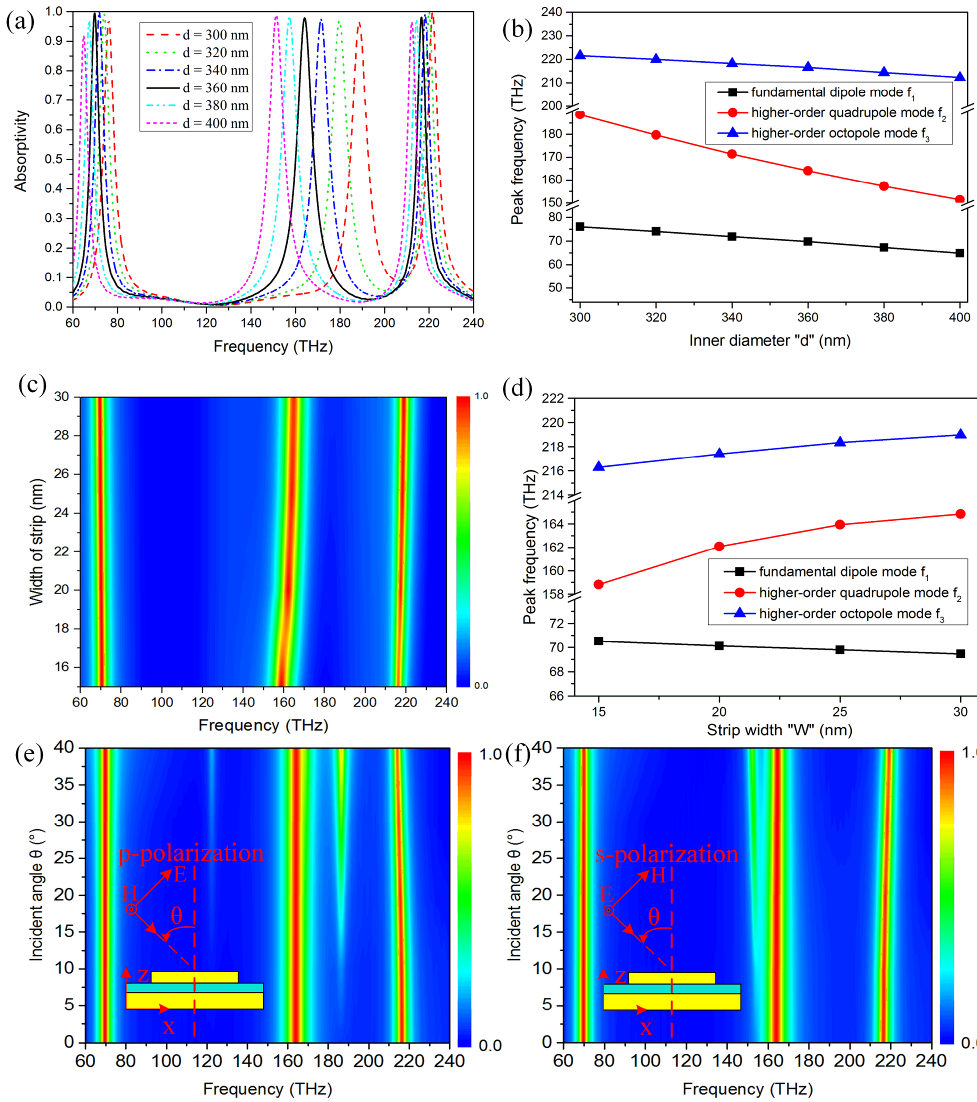

Fig. 3. (a) Spectral absorptivity and (b) absorption peaks frequency of the MPA based on the ring-strip resonators as functions of the inner diameter of the ring; (c) Spectral absorptivity and (d) absorption peaks frequency as functions of the width of the strip. The spectral absorptivity of the ring-strip structure as functions of the incident angles for (e) p-polariton waves and (f) s-polariton waves.

As shown in Fig. 2, the electric fields of the three absorption peaks all mainly accumulate around the rings and strips. So we also investigate the dependence of the absorption peaks on the inner diameter of the ring and the width of the strip. Figure 3(a) shows the dependence of spectral absorptivity on the inner diameter of the ring while other geometry parameters are kept constant. When the inner diameter "d" increases from 300 to 400 nm, our designed ring-strip structure can always excite three absorption peaks in the infrared range but the absorption peaks frequency have a little change. As shown in Fig. 3(b), the increase of the inner diameter causes the decrease of the absorption peaks frequency for both the fundamental mode and the two higher-order modes. Figure 3(c) shows the dependence of spectral absorptivity on the width of the strip while other geometry parameters are kept constant. When the width "W" increases from 15 to 30 nm, there are always three absorption

Optics EXPRESS

peaks but the absorption peaks frequency have a little change. As shown in Fig. 3(d), the increase of the width causes the decrease of the absorption peaks frequency of the fundamental electric dipole mode but the increase of the absorption peaks frequency of the higher-order electric quadrupole mode and the higher-order electric octopole mode. The Fig. 3(e) and 3(f) show the effects of the incident angles on the spectral absorptivity for p-polariton waves and s-polariton waves, respectively. The fundamental and higher-order modes all maintain high absorptivity when the incident angles increase from 0 to 40 degrees. But the absorption peaks frequency have a little change. For p-polariton waves, the absorption peaks frequency of the dipole and quadrupole modes are almost unchanged but the absorption peaks frequency of the octopole modes have a slight decrease. For s-polariton waves, the absorption peaks frequency of the dipole are almost unchanged but the absorption peaks frequency of the quadrupole and octopole modes both have a slight increase.

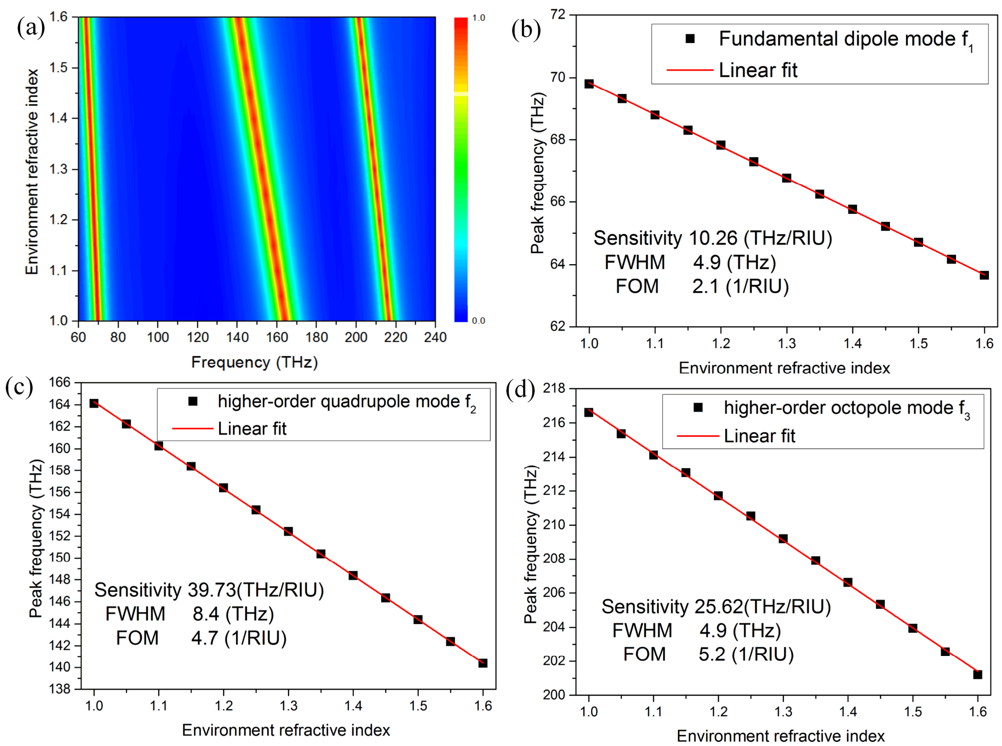

Fig. 4. (a) Spectral absorptivity of the ring-strip structure as functions of the surrounding environment refractive index increasing from 1.0 to 1.6; Absorption peaks frequency of (b) the fundamental electric dipole mode, (c) the higher-order electric quadrupole mode, and (d) the higher-order electric octopole mode shift against the surrounding environment refractive index.

In order to investigate the potential of our designed MPA based on the ring-strip structure as the biological sensor, we simulate the electromagnetic performance of the structure with an extra cladding medium layer with the refractive index increasing from 1.0 to 1.6 as shown in Fig. 4(a). When the environmental refractive index increases from 1 to 1.6, our designed ring-strip structure can always excite three absorption peaks in the infrared range. But increasing the environmental refractive index causes the decrease of the absorption peaks frequency for both the fundamental electric dipole mode and the higher-order electric quadrupole and electric octopole modes. The performance of the biological sensor usually can be evaluated by the figure-of-merit (FOM) which is defined as the ratio of refractive index sensitivity S and the full-width-half-maximum (FWHM) of the corresponding absorption peaks:

Optics EXPRESS

$$FOM = \frac{S}{FWHM} \tag{1}$$

The refractive index sensitivity S is defined as the dependence of the absorption peak frequency change Δf on the refractive index change Δn :

$$S = \frac{\Delta f}{\Delta n} \tag{2}$$

The peaks frequency of the fundamental electric dipole mode decrease as the refractive index increase as shown in Fig. 4(b). The sensitivity of the electric dipole mode is 10.26 THz/RIU which defined as the slope of the linear fitted line plotted with solid red line and the FWHM is 4.9 THz. So the FOM value is calculated as 2.1 RIU^{-1} for the fundamental electric dipole mode. The peaks frequency of the higher-order electric quadrupole mode decrease as the refractive index increase as shown in Fig. 4(c). The sensitivity of the electric quadrupole mode is 39.73 THz/RIU and the FWHM is 8.4 THz. So the FOM value is calculated as 4.7 RIU^{-1} for the higher-order electric quadrupole mode. The peaks frequency of the higher-order electric octopole mode decrease as the refractive index increase as shown in Fig. 4(c). The sensitivity of the electric quadrupole mode is 25.62 THz/RIU and the FWHM is 4.9 THz. So the FOM value is calculated as 5.2 RIU^{-1} for the higher-order electric octopole mode. From above calculation, the FOMs are 2.1, 4.7, and 5.2 RIU^{-1} for the fundamental electric dipole mode at f_1 = 69.8 THz, the higher-order electric quadrupole mode at f_2 = 164.1 THz and the higher-order electric octopole mode at f_3 = 216.6 THz, respectively. It is obvious that the sensing performance of the higher-order modes is higher than the fundamental modes [33]. And the sensing performance of our designed absorber is superior to the published work [38].

3.2 MPA based on the super resonator with six absorption bands

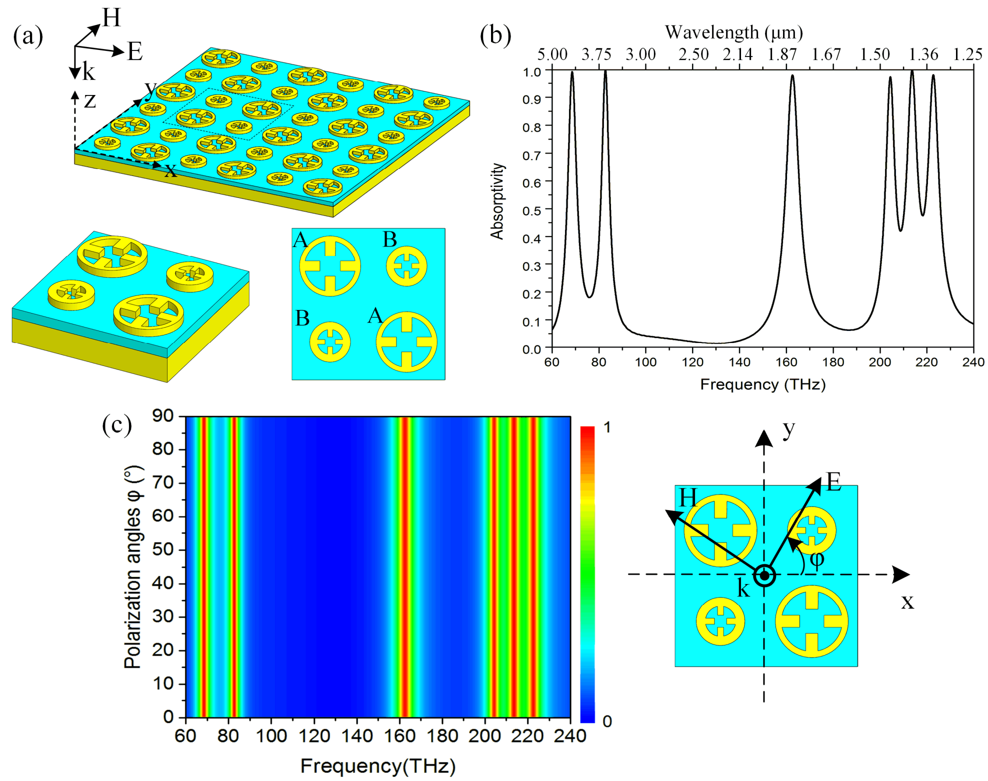

Fig. 5. (a) Schematic diagram and (b) spectral absorptivity of our designed MPA based on the super resonators consisting of two different sized basic resonators A and B. (c) The spectral absorptivity as functions of the polariton angles.

Our designed MPA based on the basic resonators can simultaneously excite the fundamental electric dipole modes at f_1 = 69.8 THz with absorptivity 99.5%, the higher-order electric quadrupole modes at f_2 = 164.1 THz with absorptivity 97.8%, and higher-order electric octopole modes f_3 = 216.6 THz with absorptivity 98.1%. To achieve more absorption bands, we design another one MPA based on the super resonators consisting of two different sized basic resonators A and B in the unit cell as shown in Fig. 5(a). The electromagnetic waves are incident vertically on the nanostructure and the electric fields are polarized in the x-direction. The optimized geometry parameters used in the simulation are as follows: P = 1.2, d_A = 0.42, d_B = 0.3, D_A = 0.5, D_B = 0.5, W_A = W_B = 0.02, and L_A = L_B = 0.05 (units: μm). The spectral absorptivity is theoretically calculated and shown in Fig. 5(b). There are totally six absorption bands in the infrared range, which are at 68.6 THz, 82.9 THz, 162.8 THz, 204.5 THz, 213.8 THz, and 222.9 THz with absorptivity 99.3%, 99.9%, 98.1%, 97.5%, 99.8%, and 98.2%, respectively. So a six-band MPA is achieved in the infrared range with average absorptivity 98.8%. Figure 5(c) shows the spectral absorptivity of the MPA based on the super resonators consisting of two different sized basic resonators A and B as functions of the polariton angles. Due to the symmetry of the structure, it's clear to see that the polariton angles have almost no effects on the absorptivity.

Optics EXPRESS

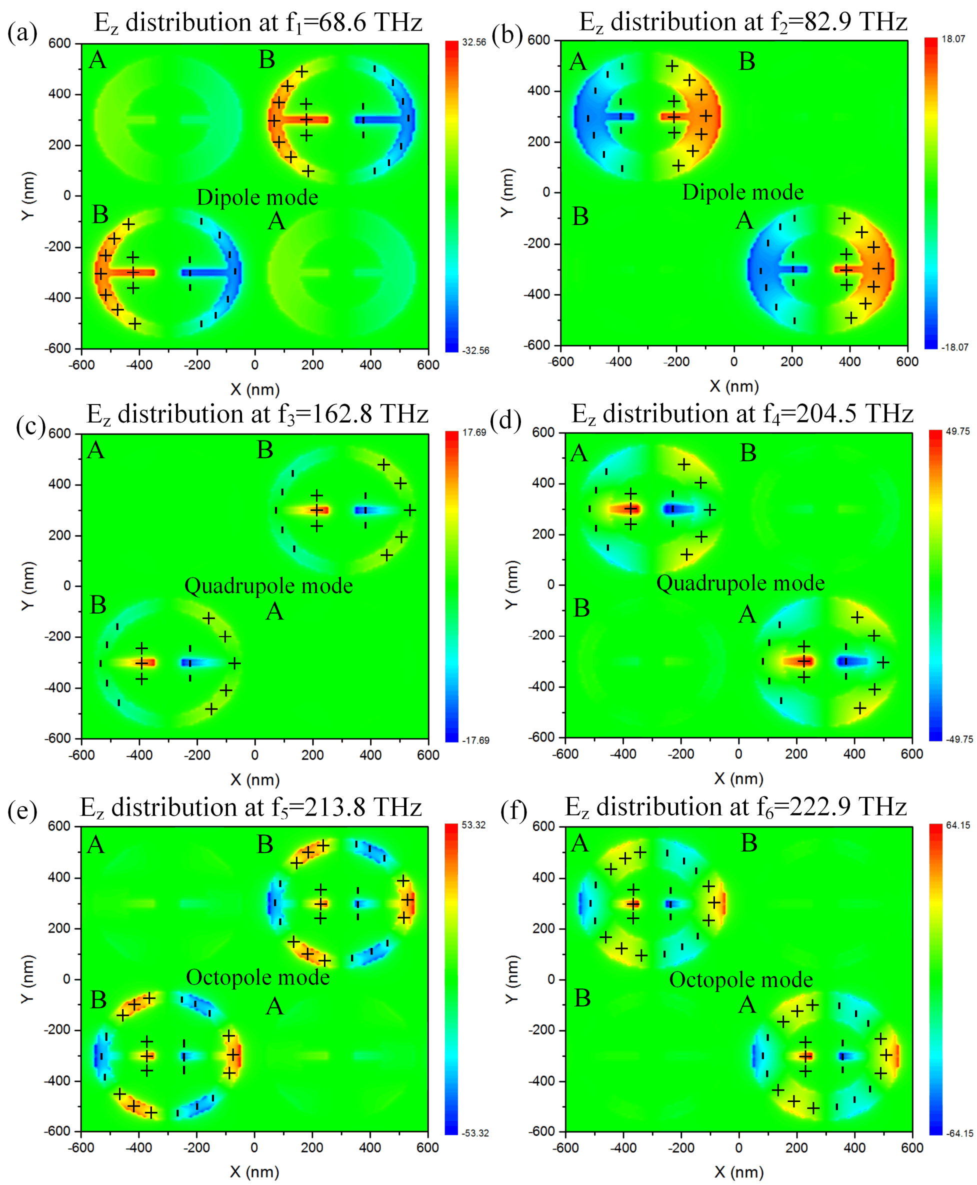

Fig. 6. The x-y cross-section view for the distribution of z component of electric fields E_z at (a) 68.6 THz, (b) 82.9 THz, (c) 162.8 THz, (d) 204.5 THz, (e) 213.8 THz, and (f) 222.9 THz.

The MPA based on the basic ring-strip structure can excite a fundamental electric dipole mode, a higher-order electric quadrupole mode, and a higher-order electric octopole mode as shown in Fig. 2. So we also calculate the z-component of electric fields distribution of the MPA based on the super resonators consisting of two different sized basic resonators A and B as shown in Fig. 6. It is obvious that there are two poles with equal magnitude but opposite signs for absorption peaks at 68.6 THz and 82.9 THz as shown in Fig. 6(a) and 6(b). The charges mainly accumulate around the B at 68.6 THz and around the A at 82.9 THz. Therefore, the absorption peaks at 68.6 THz and 82.9 THz come from the excitation of electric dipole (ED) modes of basic resonators B and A, respectively. There are four poles with equal magnitude, in which there are two positive poles and two negative poles, for absorption peaks at 162.8 THz and 204.5 THz as shown in Fig. 6(c) and 6(d). The charges mainly accumulate around the B at 162.8 THz and around the A at 204.5 THz. Therefore, the absorption peaks at 162.8 THz and 204.5 THz come from the excitation of electric quadrupole (EQ) modes of basic resonators B and A, respectively. There are eight poles with equal magnitude, in which there are four positive poles and four negative poles, for absorption peaks at 213.8 THz and 222.9 THz as shown in Fig. 6(e) and 6(f). The charges mainly accumulate around the B at 213.8 THz and around the A at 222.9 THz. Therefore, the absorption peaks at 213.8 THz and 222.9 THz come from the excitation of electric octopole (EO) modes of basic resonators B and A, respectively.

3.3 MPA based on the super resonator with twelve absorption bands

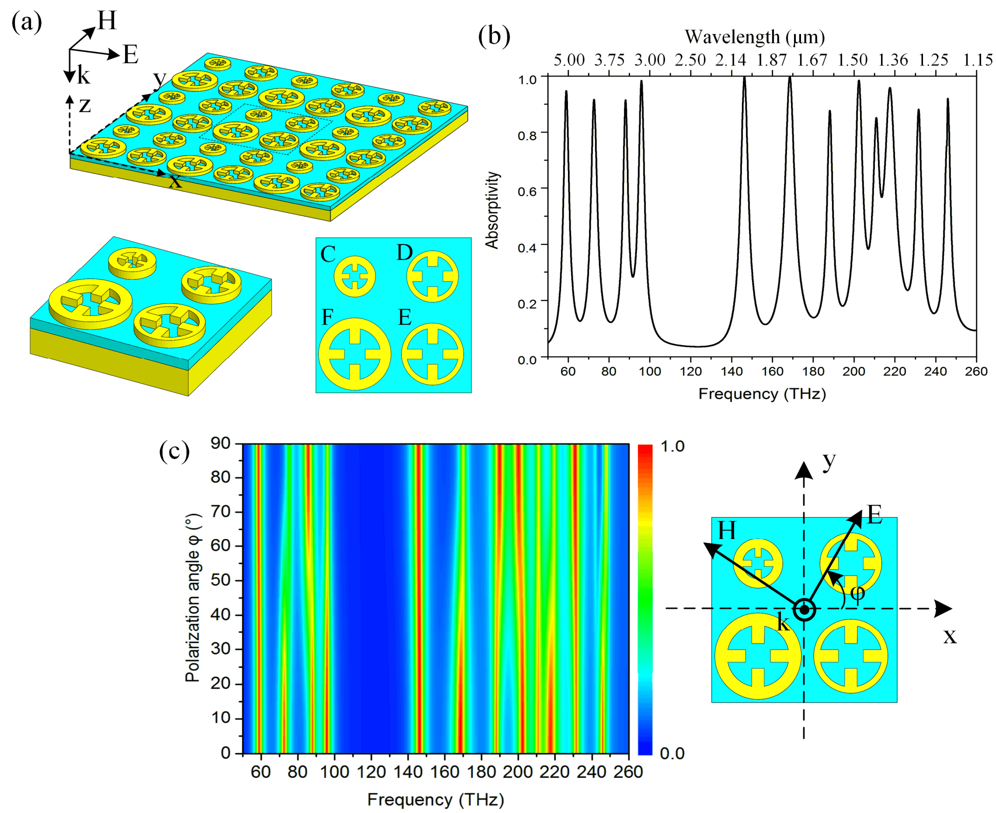

Fig. 7. (a) Schematic diagram and (b) spectral absorptivity of our designed MPA based on the super resonators consisting of four different sized basic resonators C, D, E, and F. (c) The spectral absorptivity as functions of the polariton angles.

Our designed MPA based on the basic resonators can simultaneously excite a fundamental electric dipole modes, a higher-order electric quadrupole modes, and a higher-order electric octopole modes with average absorptivity 98.5% as shown in Fig. 2. We also design one MPA based on the super resonators consisting of two different sized basic resonators A and B in one unit cell as shown in Fig. 5, which can simultaneously excite two fundamental electric dipole modes, two higher-order electric quadrupole modes, and two higher-order electric octopole modes with average absorptivity 98.8%. To achieve more absorption bands, we design another one MPA based on the super resonators consisting of four different sized basic resonators C, D, E, and F in one unit cell as shown in Fig. 7(a). The optimized geometry parameters used in the simulation are as follows: P = 1.2, d_C = 0.26, d_D = 0.3, d_E = 0.42, d_F = 0.5, D_C = 0.44, D_D = 0.48, D_E = 0.48, D_F = 0.6, W_C = 0.04, W_D = 0.02, W_E = 0.02, W_F = 0.06, L_C = 0.03, L_D = 0.03, L_E = 0.05, and L_F = 0.05 (units: μm). The spectral absorptivity is theoretically calculated and shown in Fig. 7(b). There are totally twelve absorption bands in the infrared range, which are at 59 THz, 72.6 THz, 88.1 THz, 95.8 THz, 146.3 THz, 168.5 THz, 188.2 THz, 202.3 THz, 211 THz, 217.5 THz, 231.7 THz, and 245.9 THz with absorptivity 94.8%, 91.7%, 91.5%, 98.4%, 99.8%, 99.8%, 87.8%, 98.6%, 85.2%, 95.9%, 88.2%, 92.2%, respectively. So a twelve-band MPA is achieved in the infrared range with average absorptivity 93.7%. Figure 7(c) shows the spectral absorptivity of the MPA based on the super resonators consisting of four different sized basic resonators C, D, E, and F as functions of the polariton angles. Due to the structure is asymmetric, it's clear to see that the polariton angles have apparent influence on the spectral absorptivity. These may be because the coupling between resonators is different when the polariton angles change.

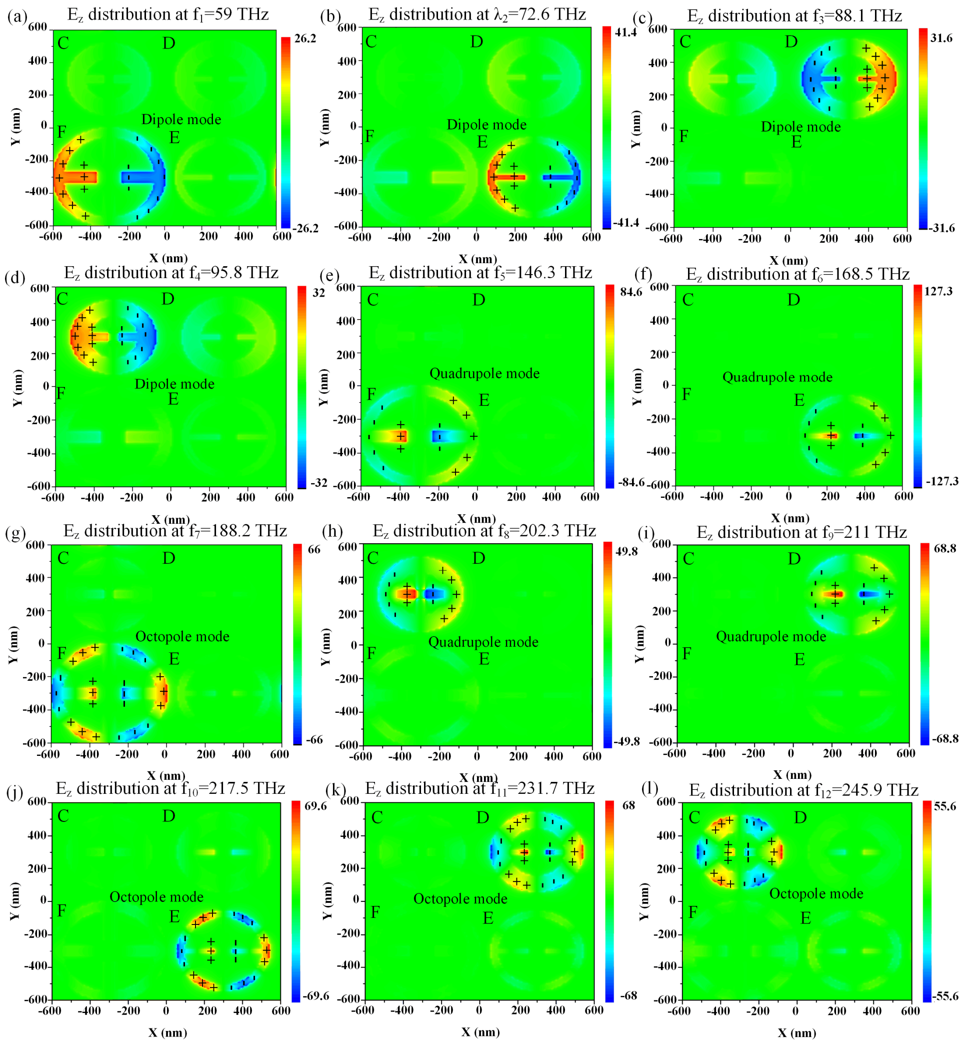

Fig. 8. The x-y cross-section view for the distribution of z component of electric fields E_z at (a) 59 THz, (b) 72.6 THz, (c) 88.1 THz, (d) 95.8 THz, (e) 146.3 THz, (f) 168.5 THz, (g) 188.2 THz, (h) 202.3 THz, (i) 211 THz, (j) 217.5 THz, (k) 231.7 THz, and (l) 245.9 THz.

To figure out the physical mechanism of the twelve absorption bands in Fig. 7(b), the z-component of electric fields distribution is plotted in Fig. 8. It is obvious that there are two poles with equal magnitude but opposite signs for absorption peaks at 59 THz, 72.6 THz, 88.1 THz, and 95.8 THz as shown in Fig. 8(a)-8(d), respectively. The charges mainly accumulate around the F at 59 THz, around the E at 72.6 THz, around the D at 88.1 THz, and around the C at 95.8 THz. Therefore, the absorption peaks at 59 THz, 72.6 THz, 88.1 THz, and 95.8 THz come from the excitation of electric dipole (ED) modes of basic resonators F, E, D, and C, respectively. There are four poles with equal magnitude, in which there are two positive poles and two negative poles, for absorption peaks at 146.3 THz, 168.5 THz, 202.3 THz, and 211 THz as shown in Fig. 8(e)-8(i), respectively. The charges mainly accumulate around the F at 146.3 THz, around the E at 168.5 THz, around the C at 202.3 THz, and around the D at 211 THz. Therefore, the absorption peaks at 146.3 THz, 168.5 THz, 202.3 THz, and 211 THz come from the excitation of electric quadrupole (EQ) modes of basic resonators F, E, C, and D, respectively. There are eight poles with equal magnitude, in which there are four positive poles and four negative poles, for absorption peaks at 188.2 THz, 217.5 THz, 231.7 THz, and 245.9 THz as shown in Fig. 8(g)-8(l), respectively. The charges mainly accumulate around the F at 188.2 THz, around the E at 217.5 THz, around the D at 231.7 THz, and around the C at 245.9 THz. Therefore, the absorption peaks at 188.2 THz, 217.5 THz, 231.7 THz, and 245.9 THz come from the excitation of electric octopole (EO) modes of basic resonators F, E, D, and C, respectively.

4. Conclusions

In summary, a triple-band MPA is designed in the infrared frequency range only utilizing single one ring-strip resonator. The absorption peaks are at f_1 = 69.8 THz, f_2 = 164.1 THz, and f_3 = 216.6 THz with absorptivity 99.5%, 97.8%, and 98.1%, respectively. The average absorptivity of those three absorption peaks reaches up to 98.5%. The absorption mechanism at f_1 = 69.8 THz, f_2 = 164.1 THz, and f_3 = 216.6 THz is attributed to the excitation of the fundamental electric dipole plasmon resonance mode, the higher-order electric quadrupole plasmon resonance mode, and the higher-order electric octopole plasmon resonance mode by analyzing the z component of electric fields distribution. As the biosensor, the FOM values are 2.1, 4.7, and 5.2 for resonant modes at f_1 = 69.8 THz, f_2 = 164.1 THz, and f_3 = 216.6 THz, respectively. It is obvious that the sensing performance of the higher-order modes is higher than the fundamental modes. A six-band MPA is achieved by combining two different sized ring-strip resonators with average absorptivity up to 98.8%, which can excite two dipole modes at 68.6 THz and 82.9 THz, two quadrupole modes at 162.8 THz and 204.5 THz, and two octopole modes at 213.8 THz and 222.9 THz. A twelve-band MPA is achieved by combining four different sized ring-strip resonators with average absorptivity up to 93.7%, which can excite four dipole modes at 59 THz, 72.6 THz, 88.1 THz, and 95.8 THz, four quadrupole modes at 146.3 THz, 168.5 THz, 202.3 THz, and 211 THz, and four octopole modes at 188.2 THz, 217.5 THz, 231.7 THz, and 245.9 THz.

Funding

National Natural Science Foundation of China (51576054).